Temperature and Intensity Dependence of the Limiting Efficiency of Silicon Solar Cells

D. Akira Engelbrecht and Thomas Tiedje

***Abstract*—The temperature and intensity dependence of the limiting efficiencies of monofacial and bifacial silicon solar cells are calculated from the physical properties of silicon assuming light trapping by Lambertian scattering from rough surfaces. The maximum efficiency of a bifacial cell (28.92%) is lower than the efficiency of a monofacial cell (29.46%) at room temperature and Air Mass 1.5 Global illumination. The effects of electron–electron interactions on the band gap, radiative recombination rate, and optical absorption are included self-consistently. The temperature coefficient of the output power is −0.23%/°C for the optimum thickness monofacial cell at room temperature. The optimum thickness of silicon solar cells decreases strongly with temperature following a power law T^{-7} and thin cells have a lower temperature coefficient than thick cells. A surface recombination velocity of 1 cm/s is found to be a turning point below which surface recombination has a small effect on the efficiency.**

***Index Terms*—Bifacial solar cells, efficiency limits, intensity dependence, silicon solar cells, surface recombination, temperature dependence.**

I. Introduction

CRYSTALLINE silicon solar panels are the dominant commercial solar cell technology, with annual sales exceeding 100 GW globally [1]. For a given insolation level, the efficiency of the solar panel determines the output power and is, therefore, a key factor in the cost of solar electricity. The maximum efficiency of silicon solar cells has been examined theoretically in detail under standard operating conditions consisting of Air Mass 1.5 Global illumination (AM1.5 G) and 25 °C operating temperature [2]–[4]. The theoretical calculations typically assume that the silicon solar cells have rough front and/or back surfaces that enhance optical absorption through light trapping. The calculation by Schäfer and Brendel [3] shows that the physical properties of silicon limit the maximum solar cell efficiency to 29.56% under standard operating conditions of AM1.5 G and 25 °C. The theoretical limiting efficiency calculations have been successful in the sense that the limit has been approached quite closely experimentally, but has not been exceeded. The record high measured efficiency for a silicon solar cell is 26.7 ± 0.5% [5], [6] or 90% of the theoretical limit. The theoretical maximum efficiency of silicon solar cells is a useful benchmark in the design of high-efficiency photovoltaic devices and for comparing the performance of silicon solar cells with photovoltaic devices made from other materials [6]. Given the growing importance of solar electricity and the dominant position of silicon, it is useful to extend the calculations of the limiting efficiency to nonstandard operating conditions.

Solar panels normally operate above ambient temperature due to heating by sunlight. According to Migan [7], the temperature of a solar panel under full solar illumination is about 20 °C above ambient, although wind reduces the temperature rise [8], [9]. Normal operating temperature is considered to be 45 °C by some manufacturers [10].

In this article, we calculate the limiting cell efficiency and optimum thickness as a function of temperature. Recently there has been growing interest in bifacial solar panels which are sensitive to light incident on both sides [11]. Therefore, we calculate the temperature and intensity dependence of the efficiency of bifacial cells as well as conventional single-sided or monofacial cells using a similar method to that used earlier [2]–[4], [12] with the latest values for the relevant material parameters. Several improvements are incorporated into the model itself including a self-consistent treatment of the effect of free carriers on the radiative recombination rate and the optical absorption and more recent data on the Auger recombination rate and free carrier absorption. We also determine the effect of surface recombination on the efficiency for values of the surface recombination velocity in the range that has been observed experimentally. As in the earlier work, we assume that the solar cells consist of silicon sheets that are roughened in order to increase the optical absorption through light scattering. Corrections associated with electron–electron interaction effects are included. Since silicon is available in the form of high purity, low defect density single crystals, we neglect nonradiative recombination at bulk crystal defects and impurities. In this article, intrinsic silicon is considered exclusively because it gives the highest efficiency.

II. Optical Absorption

Two different optical designs are considered. In the conventional, or monofacial, design, the solar cell is a one-sided device consisting of a slab of intrinsic silicon with an antireflection

Manuscript received January 21, 2020; revised March 19, 2020, May 22, 2020, July 22, 2020, and September 9, 2020; accepted October 27, 2020. Date of publication November 26, 2020; date of current version December 21, 2020. This work was supported by the Natural Sciences and Engineering Research Council of Canada. D. Akira Engelbrecht was partially supported by an NSERC Undergraduate Student Research Award. *(Corresponding author: Thomas Tiedje.)*

D. Akira Engelbrecht is with the Mechanical Engineering, University of Victoria, Victoria, BC V8W 2Y2, Canada (e-mail: akira.engelbrecht@gmail.com).

Thomas Tiedje is with the Electrical and Computer Engineering, University of Victoria, Victoria, BC V8W 2Y2, Canada (e-mail: ttiedje@uvic.ca).

Color versions of one or more of the figures in this article are available online at https://ieeexplore.ieee.org.

Digital Object Identifier 10.1109/JPHOTOV.2020.3035115

coated front surface and a perfectly reflecting back surface. The front and back surfaces of the silicon are both roughened to improve the optical absorbance by light trapping. The bifacial device on the other hand is two-sided with both the front and back surfaces roughened and antireflection coated with no back surface reflector. This simulates a bifacial solar panel with a bifaciality factor of 1 in which the efficiency is the same for illumination on either side. A bifaciality value of 80% has been reported for working solar panels [11]. Field observations with commercial solar panels show that bifacial solar cells can produce up to 30% more output power depending on the albedo of the ground and the panel mounting configuration [11].

In the single-sided solar cell, the absorbance can be approximated by [12], [13], [14]

$$A_j = \frac{4\alpha L/j}{4\alpha L/j + 1/n^2} \tag{1}$$

where $j = 1$. In the case of the bifacial device, the absorbance is also given by [1] but with $j = 2$. L is the thickness of the solar cell, $\alpha = \alpha_{\rm bb} + \alpha_{\rm fc}$ is the optical absorption coefficient, $\alpha_{\rm bb}$ is the band to band absorption and $\alpha_{\rm fc}$ is the free carrier absorption. The $\alpha_{\rm bb}$ absorption process produces electron-hole pairs, whereas the free carrier absorption α_{fc} produces hot carriers which quickly dissipate their excess energy to heat. The index of refraction is n: the index of refraction can be distinguished from the electron density, for which we use the same symbol, by the context. Equation (1) is a good approximation in the strong absorption and weak absorption limits [13].

If the rough front and back surfaces exhibit ideal Lambertian scattering, the optical absorption can be calculated exactly in the geometrical optics limit [3], [14], in principle improving on the approximations associated with (1). In this case, the absorbance for a single-sided cell in which both the front and back surfaces are Lambertian scatterers is [14]

$$A_j = \frac{1 - T^{2/j}\left(\alpha L\right)}{1 - \left(1 - \frac{1}{n^2}\right) T^{2/j}\left(\alpha L\right)} \tag{2}$$

where $j = 1$. In (2), L is the thickness of the silicon and α is the optical absorption coefficient. For the bifacial case in which there is no back surface mirror and both surfaces are rough and antireflection coated, the absorbance is also given by (2) except with $j = 2$. The angle-averaged optical transmission $T(x)$ is given by

$$T\ (x) = e^{-x}\ (1 - x) + x^2 E_1\left(x\right). \tag{3}$$

The last term in (3) includes the exponential integral $E_1(x)$, defined by

$$E_1\left(x\right) = \int_x^\infty \frac{e^{-u}}{u} du. \tag{4}$$

Although (2) may be an exact solution in the geometrical optics approximation, it is only an approximate solution of the full electromagnetic problem [15].

In the low absorption limit, the absorbance in (2) approaches the value in (1) whereas for $\alpha L > 1$, the absorbance value in (2) is slightly higher than in (1) and exponentially dependent on thickness [3]. The assumption that rough silicon surfaces can be approximated as Lambertian scatterers has been tested experimentally and found to provide a good description of experimental data [16]. Modeling the absorbance of silicon with random surface textures is discussed in more detail in [14].

Lambertian scattering is a convenient way to describe scattering from rough surfaces that can be realized experimentally, but it is not necessarily the optimum solution to maximize the absorption of solar radiation in a thin layer of silicon. Bhattacharya *et al*. [17], [18] have shown through numerical solutions of the full electromagnetic scattering problem that the absorbance can be further improved beyond the Lambertian scattering limit with resonant periodic surface patterns.

The free carrier absorption $\alpha_{\rm fc}$ includes contributions from both electrons and holes. Experimental measurements show that for wavelengths close to the silicon bandgap, the free carrier absorption as a function of photon energy, temperature, and carrier density can be parameterized as follows [19], [20]:

$$\alpha_{\rm fc} = \left(5.6 \times 10^{-9} \lambda^{2.88} n + 6.1 \times 10^{-12} \lambda^{2.18} p\right)\ T \tag{5}$$

with units cm^{-1}. In this equation, n and p are the electron and hole densities, assumed to be equal, the wavelength λ is measured in centimeters and the temperature in Kelvin.

III. Electron-Hole Recombination

We assume that the silicon is undoped and that under illumination, the electron and hole densities, n, p, are equal, and much larger than the intrinsic carrier concentration n_i or $n, p \gg n_i$. This will be the case, for example, if the silicon is weakly doped or intrinsic. We also assume that the ambipolar diffusion length of the photogenerated electrons and holes is large compared to the cell thickness so that the carrier concentration and quasi-Fermi levels are approximately constant throughout the cell. In other words, we neglect carrier concentration gradients associated with carrier diffusion to the contacts. Some carrier concentration gradient is needed to extract carriers, so this assumption can be regarded as an area for improvement in future modeling.

The electron density n and cell output voltage V are related by the following equation:

$$n\ = n_{i,\rm eff}\ \left(T, n\right) e^{\frac{qV}{2kT}} \tag{6}$$

where the carrier concentration dependence of the intrinsic carrier concentration $n_{i,\rm eff}$ is due to bandgap narrowing. The intrinsic carrier concentration $n_i = n_{i,\rm eff}\ (T, 0)$. The temperature and carrier concentration dependence of $n_{i,\rm eff}$ is given by [21], [22]

$$n_{i,\rm eff}\ (T, n) = \ 1.589 \times 10^{15}\ T^{1.706}\ e^{-\frac{E_g(T,n)}{2kT}} \tag{7}$$

where the bandgap $E_g(T, n)$, as a function of temperature and carrier concentration [23], has been determined by Wolf *et al*. [24] and Schenk [25] to be

$$E_g\ (T, n) = \ 1.206\ -\ 2.73 \times 10^{-4} T\ + BGN\left(T, n\right). \tag{8}$$

$BGN(T, n)$ is the bandgap narrowing caused by electron–electron correlation effects. A mathematical expression for $BGN(T, n)$ is available in [25], which is a small effect under

usual operating conditions. We evaluate n_i at 298.15 K using (7), (8) for low carrier concentrations where the band gap narrowing effect can be neglected and find $n_i = 8.28 \times 10^9$ cm^{-3} [24]. The estimated one standard deviation measurement accuracy of this value is 3% [21], [22].

Non-radiative recombination of electrons and holes at the surface is an important loss process in solar cells and improvement in surface passivation is a subject of active research. In the most efficient silicon solar cells, the front and back surfaces are passivated with dielectric coatings such as SiO_2, AlO_x, or SiN_x in order to minimize surface recombination. Surface recombination velocities as low as 0.3 and 0.1 cm/s have been reported for silicon passivated with AlO_x [4], [26]–[30] and amorphous hydrogenated silicon (a-Si/SiO_x/SiN_x) heterostructures, respectively [31]. The surface recombination velocity is likely to be temperature dependent. In the efficiency calculations in this article, we assume that the electrical contacts are in the form of small area contacts or surface passivating heterojunctions such as in the HIT type a-Si/crystalline silicon heterojunction cells [5], [32]. In the ideal case of small area contacts or surface passivating heterojunctions, the effect of the electrical contacts on the surface recombination can be neglected.

Auger recombination and radiative recombination are the two most important intrinsic bulk recombination mechanisms in high purity silicon. The Auger recombination rate has been measured as a function of both carrier density and temperature [4], [27], [33]. Under illumination as discussed above, we assume that the silicon is under high injection conditions in which case $n = p$, and $n = n_0 + \Delta n \gg n_o, p_0$, where n_0 and p_0 are the equilibrium carrier concentrations in the dark; Δn is the excess carrier concentration caused by the incident light. This assumption is valid for high illumination and low doping. In this limit, the measured room temperature ambipolar Auger lifetime has been parameterized in three publications [4], [27], [33]. We use the results in [4]

$$\frac{1}{\tau_A} = 2.38 \times 10^{-29}\, n^{1.93}. \tag{9}$$

The exponent in (9) is slightly less than the classical Auger exponent of two, due to electron–electron correlation effects [27]. For $n = 7 \times 10^{15}$ cm^{-3}, typical of carrier densities in solar cells at the maximum power point, the mean Auger lifetime in [4], [27], [33] is 12.0 $\pm$ 0.8 ms. The scatter in the different experimental measurements provides an estimate of the experimental uncertainty in the measured Auger recombination rate. Taking the ambipolar diffusion coefficient of electrons and holes to be 15 cm^2/s [34] and recombination lifetime to be 12 ms, we obtain a carrier diffusion length of 4 mm, well in excess of the solar cell thicknesses considered in this article. This supports our assumption that the quasi-Fermi levels are flat inside the solar cell.

We adopt the concentration dependence of the Auger rate from Veith-Wolf *et al*. [4] in (9) and take the temperature dependence from [33]. In this case, the combined temperature and concentration dependence of the Auger recombination rate is

$$\frac{1}{\tau_A} = C_A n^{1.93} \tag{10}$$

where

$$C_A = \left[\frac{1.58 \times 10^{-27}}{(T - 193)} + 3.01 \times 10^{-32}\, T\right]. \tag{11}$$

The temperature dependence of the Auger coefficient in (11) was obtained from measurements over the temperature range 243–473 K, at a carrier concentration $n = 5 \times 10^{16}$cm^{-3} [33]. We assume that the temperature dependence of the Auger coefficient in (11) is still valid for carrier densities in the wider range of $5 \times 10^{15} < n < 3 \times 10^{16}$ cm^{-3} typical of carrier concentrations in operating solar cells at the maximum power point, since we have no experimental data on the temperature dependence of the Auger coefficient at different carrier concentrations. The highest carrier densities will be present in the thinnest solar cells at the highest operating temperatures.

The radiative recombination coefficient B can be computed from $\alpha_{\rm bb}$, the interband optical absorption coefficient as a function of photon energy following the principle of detailed balance. Detailed balance requires that the generation rate of electron hole pairs by thermal blackbody radiation be equal to the radiative recombination rate. In this case [12],

$$B\, n_i^2 = 8\pi \int \alpha_{\rm bb} \frac{n^2 c}{\lambda^4} e^{-\frac{hc}{\lambda kT}} d\lambda \tag{12}$$

where the left-hand side is the radiative recombination rate and the right-hand side is the generation rate due to ambient temperature black body radiation. The "n_i" in (12) is the intrinsic electron density and the "n" in the integral is the index of refraction, which depends weakly on temperature and photon energy. Measurements of the interband optical absorption coefficient α_{bb} have been published by Green [35] for temperatures in the range -24 to $+200$ °C and also by Nguyen *et al*. [36]. Green provides an interpolation formula with tabulated coefficients so that the optical absorption can be determined for arbitrary temperatures in the -24 to 200 °C range (249–473 K) as follows:

$$\alpha_{\rm bb}\ (\lambda, T) = \alpha_{\rm bb}\ (\lambda, 300) \left(\frac{T}{300}\right)^{b(\lambda,T)} \tag{13}$$

where T is in Kelvin.

The radiative recombination rate is found experimentally to be dependent on the electron density [37]. The reason for the dependence on carrier density is that electrons and holes tend to attract each other, which enhances the radiative recombination rate. However, at high carrier densities, the Coulomb attraction is reduced by screening which tends to reduce the radiative recombination rate. At high temperatures, the thermal motion of the electrons and holes tends to diminish this screening effect. The effect of the photogenerated electrons and holes on the radiative recombination rate is described by the dimensionless parameter $B_{\rm Rel}(n, T)$ where $0 < B_{\rm Rel} < 1$ [37], [38]. The radiative recombination rate in photo-excited silicon is $B^* = B_{\rm Rel}\ B$. Experimental data on $B_{\rm Rel}$ as a function of carrier density and temperature are available for the temperature range from 101

to 393 K [37], [38]. This data has been fit by a mathematical expression by Altermatt *et al*. [38], which we use in this article.

In order to maintain the detailed balance relationship between photon emission and absorption for the photo-excited silicon, similar to (12), the band to band absorption must also be carrier concentration dependent. In the photo-excited state, the photon distribution has a nonzero chemical potential qV equal to the quasi-Fermi level separation between electrons and holes [39]. In this case, the analog of (13) for the photo-excited material is

$$B^* n^2 = 8\pi \int \alpha^*_{\rm bb} \frac{n^2 c}{\lambda^4} e^{-\frac{hc}{\lambda kT}+\frac{qV}{kT}} d\lambda \tag{14}$$

where $\alpha^*_{\rm bb}$ is the carrier-concentration-dependent optical absorption. Although the change in the optical absorption in the presence of a high density of electrons and holes will be wavelength dependent, we are not aware of measurements of the optical absorption of silicon as a function of carrier concentration, temperature, and wavelength. Therefore, we make a simple assumption namely that $\alpha^*_{\rm bb}/\alpha_{\rm bb}$ is a constant independent of wavelength in the narrow wavelength range of interest near the bandgap. With this assumption, by combining (6), (7), (12), and (14) we can solve for the excited state absorption

$$\alpha^*_{\rm bb} = B_{\rm Rel}\, e^{-\frac{BGN}{kT}} \alpha_{\rm bb.} \tag{15}$$

Equation (15) shows that the optical absorption is reduced under high injection conditions by the factor $B_{\rm Rel}$ and increased by the band gap narrowing effect BGN. The two factors are of the same order so the net effect on the absorption is smaller than $B_{\rm Rel}$ alone. Theoretical expressions are available in the literature for both parameters as a function of carrier density and temperature, which we use in this article [25], [38]. Experimental measurements of $B_{\rm Rel},\ BGN$ are generally consistent with the theoretical expressions but the accuracy of the experimental data alone is not sufficient to give a reliable estimate for $\alpha^*_{\rm bb}$ especially at the low injection levels characteristic of solar cell operation. Although neglecting the effect of carrier injection on the optical absorption entirely would have little effect on the results in this article, nevertheless we have chosen to include this effect for mathematical consistency and because the theoretical expressions for $B_{\rm Rel},\ BGN$ are available. The net effect of [15] on the efficiency is similar in magnitude to the free carrier absorption and not strongly temperature dependent.

The total absorption, including the free carrier absorption, is

$$\alpha^* = \alpha^*_{\rm bb} + \alpha_{\rm fc}. \tag{16}$$

The photo-excited electrons and holes are expected to primarily affect the absorption in the vicinity of the optical bandgap, so the correction in (15) is unlikely to be valid outside the bandgap region. This is not a concern because we are only interested in the optical absorption in the vicinity of the bandgap. The total absorbance in the presence of the electron–electron interaction effects is modified as follows:

$$A^*_j = \frac{1 - T^{2/j}\left(\alpha^* L\right)}{1 - \left(1 - \frac{1}{n^2}\right) T^{2/j}\left(\alpha^* L\right)} \tag{17}$$

where $j = 1, 2$ refers to monofacial and bifacial cells, respectively.

The principle of detailed balance also applies to the free carrier absorption process. However, photon emission from hot carriers can be ignored because hot carriers thermalize quickly to the band edge by nonradiative processes. In other words, the chemical potential describing the nonequilibrium hot carrier population is small and the out of equilibrium photons emitted by hot carriers can be ignored.

In steady state, the rate at which electron-hole pairs are generated by solar radiation is equal to the rate at which they are extracted into the external circuit plus the rate they are lost through the various recombination processes. Electrons and holes can recombine nonradiatively by Auger or surface recombination, or they can recombine radiatively. In the case of radiative recombination, the emitted photon is either reabsorbed in an interband transition creating a new electron-hole pair, in which case it is not lost, or it can be absorbed by free carriers and dissipated to heat, or it can escape from the surface of the solar cell. In steady state, the generation rate equals the loss rate of electron-hole pairs and recombination radiation, either by free carrier absorption or by escaping from the surface of the cell

$$I_{\rm sc} = I + I_{\rm Aug} + I_{\rm Rad} + I_{\rm Surf} + I_{\rm fc}. \tag{18}$$

The first term in (18) $I_{\rm sc}$ is the short circuit current, and the second term I is the current flowing into the external circuit. The short circuit current is obtained by integrating the product of the solar flux $\phi_G(\lambda)$ and the optical absorbance $A^*_1(\lambda)$ as a function of wavelength λ as follows:

$$I_{\rm sc,1} = q \int_{280{\rm nm}}^{1450{\rm nm}} \phi_G\left(\lambda\right) \frac{\alpha^*_{bb}}{\alpha^*} A^*_1 d\lambda \tag{19}$$

where the subscript 1 refers to the monofacial (single-sided) solar cell configuration. We note that $I_{\rm sc}$ in (19) depends on carrier density for $V > 0$. A similar expression applies for bifacial cells. The long-wavelength limit in the integral is set by the band to band optical absorption in silicon which goes to zero at long wavelengths. The factor $\alpha^*_{\rm bb}/\alpha^*$ takes into account the fact that not all of the absorbed photons create electron-hole pairs, some of the absorbed photons create hot electrons [3].

The other loss terms in (18) are the Auger recombination $I_{\rm Aug}$, surface recombination $I_{\rm Surf}$, free carrier absorption $I_{\rm fc}$, and radiative emission from the solar cell $I_{\rm Rad}$. The Auger recombination rate expressed as a current is obtained from (10), (11)

$$I_{\rm Aug} = qLC_A n^{2.93} \tag{20}$$

and the surface recombination rate is given by

$$I_{\rm Surf} = 2qSn \tag{21}$$

where S is the surface recombination velocity assumed to be the same on both faces of the solar cell.

The rate at which the recombination radiation leaks out of the surface of the cell can be calculated from the reverse process namely the rate at which external blackbody radiation is absorbed in the solar cell [3]. We take into account the high density of recombination radiation inside the cell relative to thermal equilibrium by including the photon chemical potential qV in the expression for the external blackbody radiation [39].

To simplify the integrals, we introduce the following expression for the blackbody photon flux per unit solid angle in free space:

$$b\ (\lambda, V) = \frac{2c}{\lambda^4}\, e^{-\frac{hc}{\lambda kT}+\frac{qV}{kT}}. \tag{22}$$

With this notation, the recombination radiation flux that is emitted from the surface of the solar cell, expressed as a current, for monofacial and bifacial solar cells is

$$I_{\mathrm{Rad},\,j} = j\pi q \int \frac{\alpha^*_{bb}}{\alpha^*} A^*_j b d\lambda. \tag{23}$$

Recombination radiation can escape from both the front and back surfaces of the bifacial cell ($j = 2$), which accounts for the extra factor of two in this case. Strictly speaking, the blackbody radiation flux in (23) should be the net flux $b(\lambda, V) - b(\lambda, 0)$; however, the equilibrium flux in the dark $b(\lambda, 0)$ is much smaller than $b(\lambda, V)$ at open circuit or the maximum power point and is neglected.

The rate at which recombination radiation is generated per unit volume is given by (14). Some of this radiation escapes out the surface(s) of the solar cell and is lost, as described by (23). The remainder of the radiation is absorbed either through interband transitions that create new electron-hole pairs or through free carrier absorption. The absorbed radiation can be computed by subtracting the radiation escaping from the cell in (23) from the total radiation emitted in the radiative recombination process in (14) for the monofacial and bifacial cells

$$I_{\mathrm{Abs},j} = j\pi q \int \frac{\alpha^*_{bb}}{\alpha^*} \left(4\alpha^* n^2 L/j - A^*_j\right) b\, d\lambda. \tag{24}$$

The absorption in (24) is a combination of band to band transitions and free carrier absorption. The band-to-band part of the absorption is not a loss process because it produces new electron-hole pairs and has been referred to as photon recycling [40]. The free carrier part of the absorption, which is a loss process, is a fraction of the absorption given by

$$I_{\mathrm{fc},j} = j\pi cq \int \frac{\alpha_{fc}}{\alpha^*} \frac{\alpha^*_{bb}}{\alpha^*} \left(4\alpha^* n^2 L/j - A^*_j\right) b\, d\lambda. \tag{25}$$

The factor $\alpha^*_{\mathrm{fc}}/\alpha^*$ is the fraction of the total absorbed photons that are absorbed by free carriers as discussed above. The photon current that is recycled into the band to band absorption can be obtained by replacing $\alpha_{\mathrm{fc}}/\alpha^*$ in (25) with $\alpha^*_{\mathrm{bb}}/\alpha^*$

$$I_{\mathrm{Recyc},j} = j\pi q \int \left(\frac{\alpha^*_{\mathrm{bb}}}{\alpha^*}\right)^2 \left(4\alpha^* n^2 L/j - A^*_j\right) b\, d\lambda. \tag{26}$$

For a better physical understanding of (24)–(26), it is helpful to substitute the approximate expressions for the absorbance from (1).

IV. Solar Cell Performance

Equation (18) is solved numerically for the current I, voltage V, and maximum output power using MATLAB. The maximum power point is found by iteratively solving $P = IV$ where I and V are expressed as a function of n until the maximum power condition $dP(n)/dn = 0$ is reached. The current and voltage at the maximum power point are I_{mp}, $V_{\mathrm{mp},}$ respectively. A similar approach is taken to solve for the open-circuit voltage, V_{oc}. V_{oc} is found by iteratively solving $P = IV$ for the open-circuit condition where $P(n) = 0$ and $n \neq n_i$. All integrations were performed using MATLAB's implementation of trapezoidal integration. The short circuit current I_{sc}, was calculated using the AM1.5 G 37° tilt, reference solar spectrum generated according to the ASTM specifications [41]. The spectrum was multiplied by 0.9971 so that the integrated solar flux is 100 mW/cm^2 in the wavelength range from 280 to 4000 nm. The absorption coefficients and index of refraction of silicon were interpolated to the wavelength values of the AM1.5 G solar spectrum using MATLAB's implementation of piecewise cubic interpolation. The fill factor is defined as $\mathrm{FF} = I_{\mathrm{mp}}V_{\mathrm{mp}}/I_{\mathrm{sc}}V_{\mathrm{oc}}$ and the efficiency is $\eta = I_{\mathrm{mp}}V_{\mathrm{mp}}/100$ mW.

For the intensity dependence, we used the Air Mass 1.5 Direct solar spectrum [41], multiplied by a dimensionless constant C between 10^{-3} and 10^3. The total incident intensity was calculated from

$$P_{\mathrm{total}} = C \int_{280\mathrm{nm}}^{4000\mathrm{nm}} \frac{hc}{\lambda} \phi_D\,(\lambda)\, d\lambda. \tag{27}$$

In this case, $\phi_D(\lambda)$ is the part of the solar spectrum in the direct beam of the sun. The upper and lower bounds on the integral are artificial but there is only a very small fraction of the solar spectrum outside this wavelength range.

Values for the efficiency of monofacial silicon solar cells at room temperature (25 °C = 298.15 K) and AM1.5 G taken from the literature are shown in Table I. The first row in Table I is Richter *et al.*'s [2] results for the limiting efficiency using up-to-date (2013) values for the material parameters and including the electron-electron interaction effects that reduce the bandgap and radiative recombination rate and modify the Auger recombination rate. The second row contains the device parameters for the record-setting silicon solar cell of Yoshikawa *et al*. [5], with the highest measured efficiency to date under standard conditions. Schäfer and Brendel [3] calculated the limiting efficiency using a similar method to Richter *et al*. [2] except that the improved approximation for the optical absorbance in (2) was used. Our results for monofacial cells, which are shown in Table II, are similar to Schäfer and Brendel's results as expected. We find an optimum thickness of 99.9 μm, close to the 98.1 μm found in [3]. The small reduction in efficiency relative to [3] is due to the slightly larger Auger recombination rate in [4] compared with [27]. Other changes, namely the use of a more recent higher value for the free carrier absorption [20], and the carrier density-dependent band-to-band absorption have a small effect on the efficiency and contribute fractionally to the fourth significant figure in the efficiency.

The final row in Table I is the theoretical calculation by Bhattacharya and John [17] for a silicon solar cell with a periodic surface texture tuned to resonantly enhance the optical absorption in the vicinity of the band edge. The resonant enhancement allows the optical absorption to exceed the absorption enhancement produced by scattering from random surface textures. The enhanced absorption in the band edge region means that the solar cell can be thinner, which increases the electron-hole pair concentration and hence the output voltage.

TABLE I
CALCULATED AND MEASURED SILICON SOLAR CELL PERFORMANCE PARAMETERS FROM THE LITERATURE

	L (μm)	η (%)	I_{sc} (mA/cm^2)	V_{oc} (mV)	V_{mp} (mV)	FF (%)
Richter [2]	110	29.43	43.31	761.3	697.3	89.26
Yoshikawa [5]	165	26.7±0.5	42.65	738		84.9
Schäfer [3]	98.1	29.56	43.36	763.3	699.3	89.31
Bhattacharya [18]	15	31.07	44.39	794.0		88.17

TABLE II
CALCULATED MONOFACIAL AND BIFACIAL SILICON SOLAR CELL PERFORMANCE PARAMETERS

	L (μm)	η (%)	I_{sc} (mA/cm^2)	V_{oc} (mV)	V_{mp} (mV)	FF (%)
Monofacial						
298.15 K	99.9	29.46	43.38	760.4	696.6	89.34
S=0.1 cm/s	119.9	29.32	43.56	757.1	692.4	88.90
240 K	475.4	33.35	43.75	833.2	777.0	91.52
400 K	13.5	22.58	42.60	625.9	552.3	84.67
x1000	189.6	34.46	39.66 x 10^3	859.9	798.0	90.95
Bifacial						
298.15 K	195.3	28.92	43.32	749.0	685.1	89.13
S=0.1 cm/s	226.3	28.80	43.47	746.4	681.7	88.78
240 K	943.5	32.90	43.72	823.6	767.0	91.35
400 K	26.0	21.88	42.48	610.9	537.7	84.31
x1000	370.9	33.94	39.62 x 10^3	849.6	787.4	90.78

Solar cell performance was calculated for the temperature range from 240 to 400 K. The lower limit is an extrapolation of measurements of the optical absorption as a function of temperature which extends down to 249 K [35] and the experimental data on the temperature dependence of the Auger recombination which has a lower limit of 243 K [33]. On the high-temperature side, the experimental data on which $B_{\rm Rel}$ is based stops at 393 K [37] and the free carrier absorption measurements go up to 372 K [19]. The last two parameters are relatively small effects so it is reasonable to extrapolate them to higher temperatures since the more critical parameters namely optical absorption and Auger recombination data are available up to 473 K [33],[35]. The temperature range 240–400 K covers most of the range over which commercial silicon solar panels are normally specified for operation, namely from -40 to $+85$ °C (233–358 K) [10].

The first row in Table II shows the optimum thickness and electrical output parameters for a monofacial silicon solar cell under standard conditions. The remaining four rows in Table II show the effects of surface recombination with $S = 0.1$ cm/s, of varying the operating temperature from 240 to 400 K, and of increasing the AM1.5 Direct radiation by a factor of 1000, with all other operating parameters kept at the reference values. Analogous results for bifacial cells are also shown in Table II.

A number of observations can be made. The optimum thickness of the bifacial cell is almost exactly twice the thickness of the optimum monofacial cell, as explained in the Appendix. According to (1), in the long-wavelength limit, a bifacial cell will have the same optical absorbance as a monofacial cell with half the thickness. As a result, the short circuit currents for the monofacial and bifacial cells in Table II are almost identical. The larger thickness of the bifacial cell reduces the output voltage and reduces the efficiency by 0.54% absolute or 1.8% relative. A surface recombination velocity of 0.1 cm/s on both front and back surfaces has only a small effect on the efficiency (-0.5% relative). The optimum thickness decreases strongly with operating temperature and increases when surface recombination is present.

In line with convention in the literature [2], [3], the limiting efficiency in Table II is presented with four significant digits. Since Auger recombination is the most important loss process, it is reasonable to expect the measurement uncertainty in the value of Auger recombination rate to have an important effect on the accuracy of the calculated efficiency. As discussed above, under typical conditions, the experimental Auger lifetime is 12.0 ± 0.8 ms. This uncertainty in the Auger coefficient leads to uncertainty in the efficiency of $29.46 \pm 0.045\%$.

The intrinsic carrier concentration at room temperature n_i determines the relationship between the output voltage and the carrier density. The experimental uncertainty in this quantity is $\pm 3\%$ [21], [22] which produces uncertainty in the efficiency of $29.46 \pm 0.060\%$. Combining the two uncertainties leads to the result that the limiting efficiency of the monofacial solar cell is $29.46 \pm 0.08\%$ including the experimental error in the intrinsic carrier concentration and Auger recombination rate. Failures of the optical absorption model to correctly describe the light scattering associated with a random surface texture and experimental uncertainties in the electron–electron interaction effects are difficult to quantify and not included.

Table III shows how the various loss processes change for the different operating conditions included in Table II. We note that the carrier density at the maximum power point does not

TABLE III
CARRIER DENSITIES AND LOSSES AT MAXIMUM POWER POINT IN MONOFACIAL AND BIFACIAL SILICON SOLAR CELLS

	n_{mp} (10^{15} cm^{-3})	I_{Aug} (mA/cm^2)	I_{Rad} (mA/cm^2)	I_{Surf} (mA/cm^2)	I_{fc} (mA/cm^2)
Monofacial					
298.15 K	6.81	0.943	0.129	0	0.0052
S=0.1 cm/s	6.26	0.887	0.123	0.201	0.0055
240 K	2.94	0.651	0.150	0	0.0100
400 K	17.3	1.610	0.116	0	0.0022
x1000	54.2	783	7.47	0	4.53
Bifacial					
298.15 K	5.41	0.939	0.162	0	0.0052
S=0.1 cm/s	5.06	0.894	0.157	0.162	0.055
240 K	2.31	0.637	0.187	0	0.0100
400 K	13.9	1.632	0.148	0	0.0022
x1000	43.4	796	10.21	0	4.94

Thicknesses are in Table II.

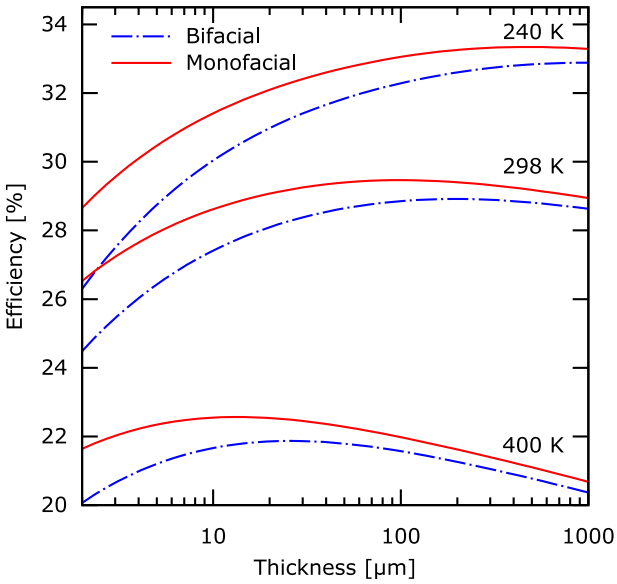

Fig. 1. Efficiency as a function of thickness at 240, 298, and 400 K for AM1.5 G illumination, neglecting surface recombination. The solid lines are for monofacial cells and the broken lines for bifacial cells.

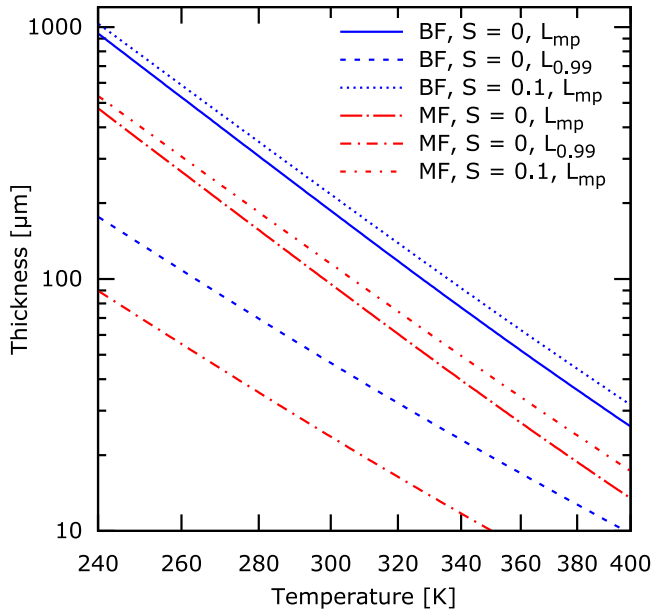

Fig. 2. Optimum thickness as a function of temperature for mono and bifacial cells, as indicated in the legend, for AM1.5 G illumination with surface recombination velocities $S = 0$ and 0.1 cm/s. Both axes are log scales. The two lower broken lines show the thickness values where the efficiency drops to 99% of the peak efficiency at the optimum thickness. These lines show how much the thickness can be reduced without significant loss in efficiency.

change very much with temperature. Even a small increase in carrier concentration with temperature would be expected to significantly increase the Auger losses, due to the exponent 2.93 in the Auger recombination rate. However, the decrease in thickness with increasing temperature compensates for the increase in recombination per unit volume, so that the total Auger losses don't change very much with temperature. Nevertheless, Auger recombination is the dominant loss process under all operating conditions in Table III. Extrapolating the surface recombination to $S = 1$ cm/s suggests that surface recombination will exceed Auger as the dominant loss process when $S > 1$ cm/s. Even for small surface recombination velocities, surface recombination exceeds radiative losses. Free carrier absorption is small in all cases, even at high temperatures and high solar concentration.

TABLE IV
FITTING PARAMETERS FOR OPTIMUM THICKNESS AS A FUNCTION OF TEMPERATURE

	a	***b***
MF	2.098×10^{19}	6.998
BF	5.714×10^{19}	7.056

$R^2 = 0.9997$.

V. TEMPERATURE DEPENDENCE

In this section, we show how the limiting efficiency of silicon solar cells depends on temperature, thickness, and surface

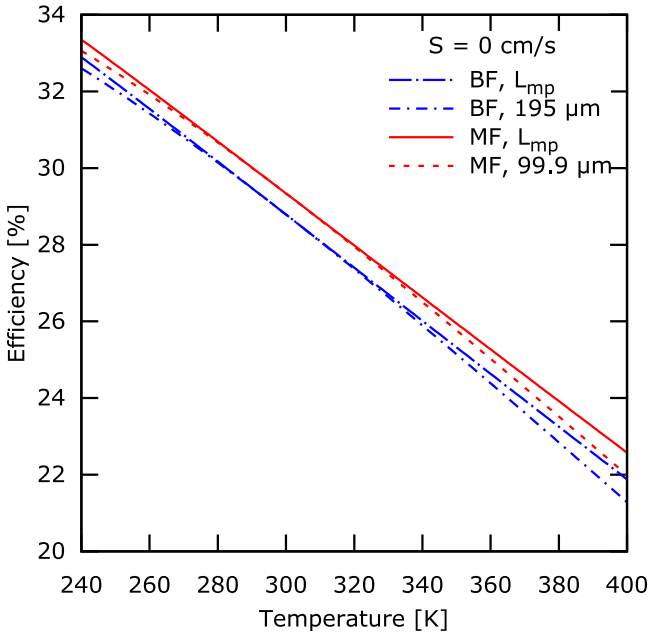

Fig. 3. Efficiency for mono and bifacial cells as a function of temperature for the optimum thickness at each temperature and for a fixed thickness equal to the optimum at 298 K. The illumination is AM1.5 G and surface recombination is neglected.

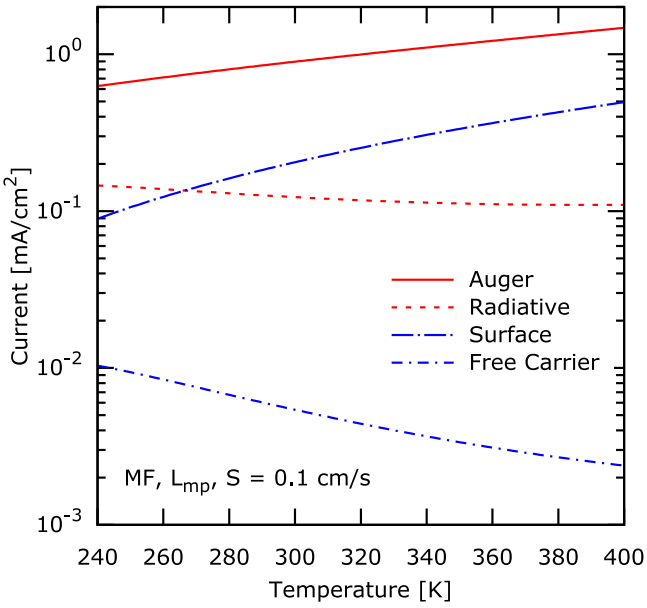

Fig. 5. Losses as a function of temperature expressed as current, for a monofacial cell at the optimum thickness at each temperature for AM1.5 G and a surface recombination velocity S = 0.1 cm/s. Auger recombination is the most important loss mechanism at all temperatures.

TABLE V
FITTING PARAMETERS FOR LIMITING EFFICIENCY AS A FUNCTION OF TEMPERATURE

	a	*b*	*c*
MF	43.62	0.0281	6.53×10^{-5}
BF	43.49	0.0294	6.57×10^{-5}

$R^2 = 0.99996$.

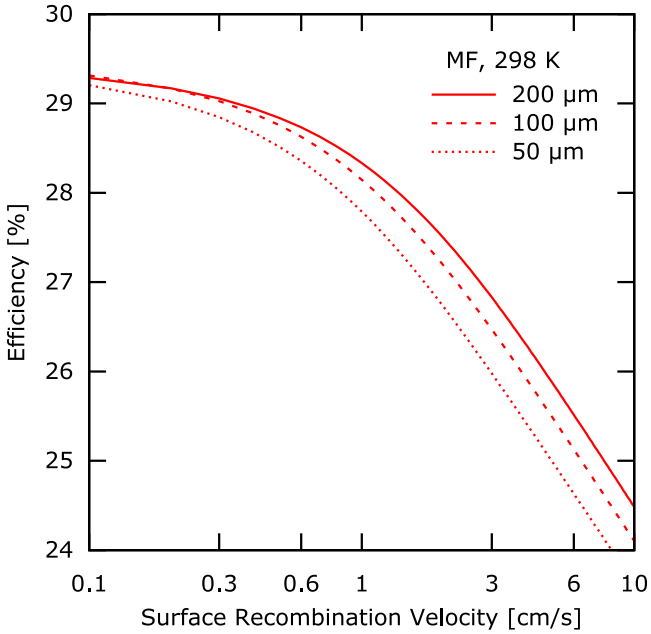

Fig. 4. Efficiency of 50, 100, and 200 μm thick monofacial solar cell as a function of surface recombination velocity at 25 °C and AM1.5 G.

recombination. Fig. 1 shows the efficiency as a function of thickness for monofacial and bifacial solar cells at three different temperatures. There is an optimum thickness because if the silicon is too thin, the cell does not absorb the light and if it is too thick, the carrier concentration drops and the output voltage goes down. The efficiency is rather insensitive to thickness near the optimum. The reason why the optimum thickness decreases with temperature can be explained as follows. The short circuit current is a strong function of thickness at small values of L but saturates at large values of L and is only weakly dependent on temperature. The open-circuit voltage, on the other hand, depends rather strongly on thickness and temperature as shown in Table II and there is no saturation. According to (6), $V 2kTln(n)$ so that $dV/dL(2kT/n)dn/dL$. If the fractional change in photogenerated carrier density with thickness, $(1/n)dn/dL$, is weakly dependent on temperature, then the thickness dependence of the output voltage increases linearly with temperature. This means that the maximum power point will shift to progressively smaller thicknesses at high temperature, due to the stronger L dependence of the voltage at high temperature and the weak L dependence of the current.

Fig. 2 is a log-log plot of the optimum silicon thickness as a function of temperature for monofacial and bifacial solar cells. The optimum thickness decreases by almost an order of magnitude from 184 μm at 0 °C to 19 μm at 100 °C. To a good approximation, it follows a power law of the form $L = aT^{-b}$. The a, b parameter values are given in Table IV: MF, BF mean monofacial, and bifacial, respectively.

When surface recombination is present, the optimum thickness increases because the surface recombination is a smaller fraction of the total recombination when the volume of the

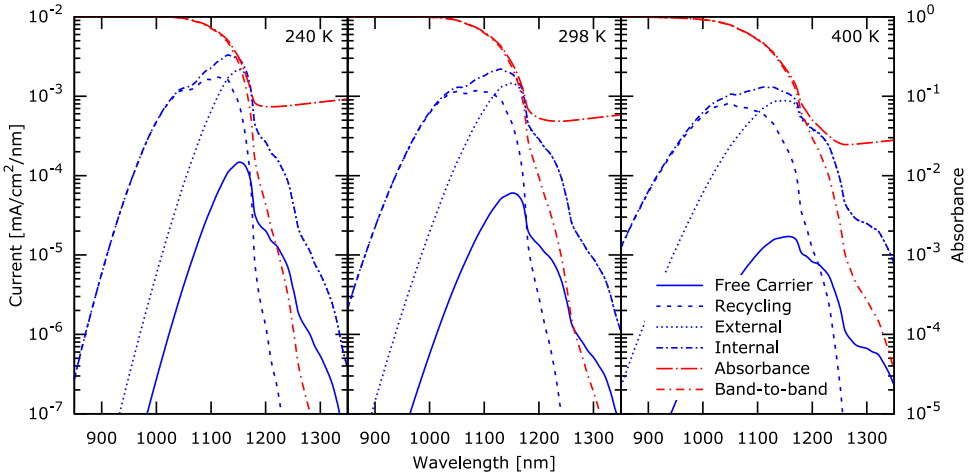

Fig. 6. Spectrum of recombination radiation that is emitted from the front surface of the cell (dotted line), the recombination radiation that is recycled in band-to-band transitions to produce new electron hole pairs (dashed line) and free carrier absorption (solid line) for a monofacial Si solar cell with the optimum thickness at 240, 298, and 400 K under AM1.5 G illumination. Also shown is the total absorbance and the band-to-band absorbance (right hand scale). The free carrier absorbance goes down at high temperatures even though the free carrier absorption per unit volume goes up because the optimum solar cell is much thinner at high temperature. See Table II for thicknesses.

silicon is larger. To illustrate the relative insensitivity of the efficiency to the solar cell thickness near the optimum, the lower dashed line in Fig. 2 shows the thickness for a 1% reduction in relative efficiency (e.g., from 29.46% to 29.17%). At room temperature, a thickness near the midpoint between the solid line and the dashed line at 50 μm would have a monofacial efficiency of about 99.75% of the maximum, assuming the efficiency as a function of thickness is a parabola. Similar reasoning applied to bifacial cells suggests their thickness could be reduced to about 65 μm with very little impact on the limiting efficiency. We conclude that significant reductions in solar cell thicknesses are possible in principle without much loss in output power from the current commercial norm of 160–170 μm [42].

Fig. 3 shows the maximum efficiency as a function of temperature for monofacial and bifacial solar cells. The solid and long dashed lines are the efficiencies for solar cells with the optimum thickness at each temperature. The broken lines show the efficiency for fixed thicknesses, equal to the optimum thicknesses at room temperature for the monofacial and bifacial cells. As expected, the broken lines are tangential to the solid and long dashed lines at room temperature. The temperature dependence of the efficiency for monofacial and bifacial cells 99.9 and 195.3 μm thick, respectively, can be described by the quadratic equation, $\eta(\%) = a - bT - cT^2$ with fitting parameters a, b, c provided in Table V.

The efficiency of a monofacial solar cell at room temperature as a function of surface recombination velocity is shown in Fig. 4 for three different cell thicknesses. As expected surface recombination has a more detrimental effect on the efficiency of thin cells. Once the surface recombination velocity is less than $\sim$1 cm/s, the efficiency is weakly dependent on surface recombination.

Fig. 5 shows the temperature dependence of the four-loss processes considered in this article for monofacial cells with the optimum thickness at each temperature and a surface recombination velocity of 0.1 cm/s. Auger recombination is the most important loss, and free carrier absorption is small. At room temperature for $S = 0.1$ cm/s the loss due to surface recombination is similar to the radiative emission loss and much smaller than the Auger loss.

Fig. 6 shows the spectral dependence of the internal recombination radiation and the part of this radiation that leaves the cell and the part that is reabsorbed for $T = 240$, 298, and 400 K for a monofacial cell with the optimum thickness at each temperature obtained from (14), (23), (25), and (26). Fig. 6 also shows the spectral dependence of the absorbance at different temperatures. The short wavelength part of the emission spectrum tends to be reabsorbed, whereas the long wavelengths have a higher probability of escaping from the cell, as one would expect. Although the width of the spectrum increases with temperature, the total intensity of the recombination radiation is relatively insensitive to temperature.

Fig. 7 shows the short circuit current, open-circuit voltage, and fill factor as a function of temperature for monofacial and bifacial cells for the optimum thickness at each temperature and fixed thicknesses equal to the optimum thicknesses at room temperature. The short circuit current increases with temperature for the fixed thickness cells because the optical bandgap of silicon decreases and the silicon is more strongly absorbing. The short circuit current decreases with temperature for optimum thickness cells because the thickness of the silicon decreases rapidly with temperature which reduces the absorbance, even though the bandgap shrinks. We note that the open-circuit voltage has a stronger temperature dependence than the short circuit current or the fill factor.

The results in this article can be compared with the temperature dependence of the performance of commercial solar panels [43]. A silicon heterojunction panel with an open-circuit voltage of 732.5 mV and efficiency of 21.4% at room temperature

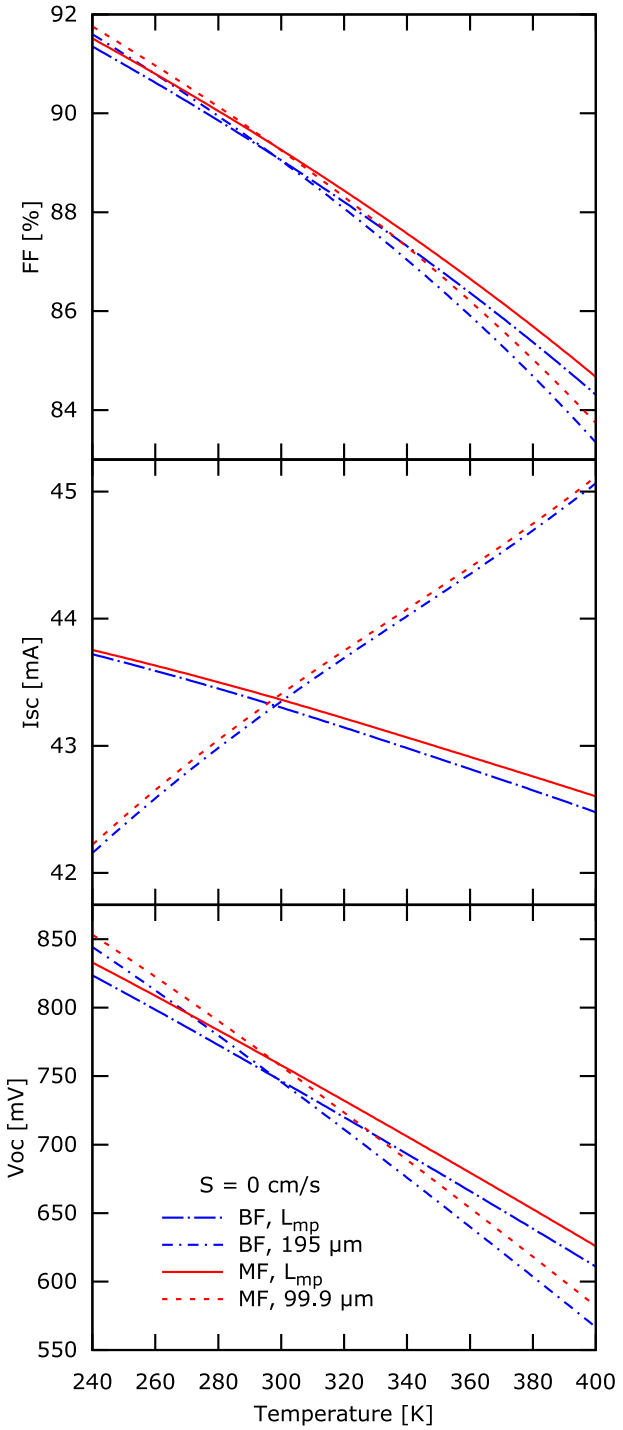

Fig. 7. Fill factor, short circuit current, and open circuit voltage as a function of temperature for mono and bifacial cells under AM1.5 G illumination for the optimum thickness at each temperature as well as for a fixed thickness equal to the optimum room temperature thickness with S = 0.

was observed to have a temperature coefficient $dV_{\rm oc}/dT = -1.6\ {\rm meV/K}$ [43]. According to the theory presented here, a solar cell with this output voltage and $S = 0$ will have a temperature coefficient of $-1.8\ {\rm meV/K}$. A detailed comparison is presented in a separate publication [44].

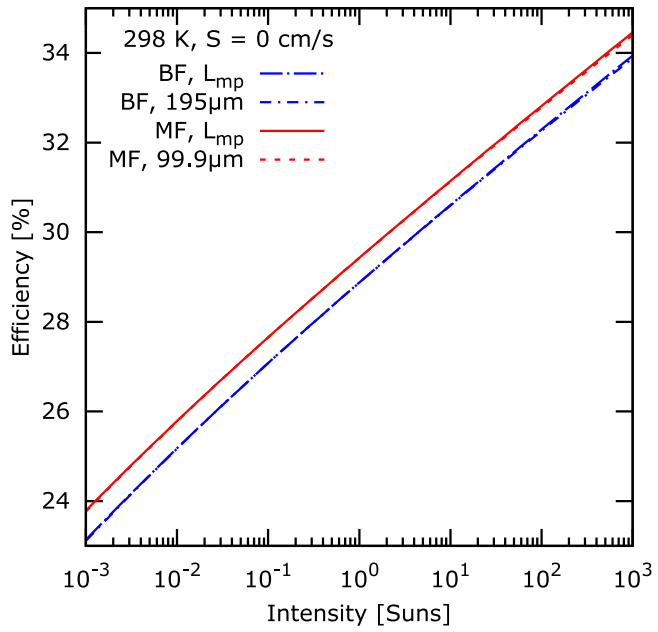

Fig. 8. Intensity dependence of the efficiency for mono and bifacial solar cells at room temperature, for S = 0. Only the direct component of the AM1.5 G solar spectrum is used in the calculation of the short circuit current. The optimum thickness increases with intensity (see Table II) which explains why the fixed thickness and optimum thickness curves are slightly different.

TABLE VI
FITTING PARAMETERS FOR INTENSITY DEPENDENCE OF EFFICIENCY AT 25 °C.

	η_{1Sun}	b	c	$\frac{1}{\eta}\frac{d\eta}{d(logI)}$ at $C = 1$
MF	29.43	1.758	-0.0377	5.88 (%/dec.)
BF	28.88	1.780	-0.0415	6.15 (%/dec.)

The MF and BF Cells are 99.9 and 195.3 μm thick, respectively. $R^2 = 0.99996$.

VI. INTENSITY DEPENDENCE

Fig. 8 shows the efficiency as a function of intensity for the AM1.5 Direct illumination spectrum [41] for monofacial and bifacial cells for a fixed thickness and the optimum thickness at each intensity, at room temperature. The intensity dependence is obtained by multiplying the AM1.5D spectrum by a dimensionless constant C between 0.001 and 1000. The efficiency as a function of intensity at room temperature can be fit with the equation, $\eta\ (C) = \eta_{1Sun} + b(logC) + c(logC)^2$ where the dimensionless intensity $C = 1$ is defined as an intensity of one sun for AM1.5D [41]. The fitting parameters η_{1Sun}, b, c are given in Table VI. The efficiency at one sun in Table VI is slightly lower than in Table II because AM1.5D has a lower intensity than AM1.5 G.

At one sun, the relative efficiency of a monofacial cell increases by 5.88%/decade, as shown in Table VI. The efficiency is a stronger function of intensity at low intensities reaching 8.2%/decade for a monofacial solar cell at 0.001 suns. This is similar to the 8.5%/decade found earlier for the efficiency at low intensities [45]. Using the fitting parameters, we find that the efficiency of a bifacial cell at a concentration factor of two is equal to the efficiency of a monofacial cell for a concentration

of one. This is expected because for a concentration of two the electron density of the bifacial cell is approximately the same as a monofacial cell for a concentration of one since the bifacial cell is twice as thick and has the same absorbance.

VII. Conclusion

Numerical calculations of the maximum efficiency of silicon solar cells that is allowed by the physical properties of silicon have been extended to non-standard operating conditions and bifacial solar cells. The efficiency of single-sided (monofacial) and doubled-sided (bifacial) devices has been calculated as a function of temperature, intensity, and surface recombination velocity for cells in which Lambertian light scattering from rough surfaces is used to enhance the optical absorbance. The effect of electron–electron interactions on the radiative recombination coefficient and the optical absorption is treated self consistently. The room temperature efficiency for monofacial cells ($29.46 \pm 0.08\%$) is in good agreement with earlier work and the efficiency for bifacial cells is found to be slightly lower than for monofacial cells (28.92%). Provided the surfaces are passivated against surface recombination and recombination at contacts is small, Auger recombination is the dominant loss mechanism at all temperatures in the range 240 to 400 K. Once the surface recombination velocity is reduced below about $\sim$1 cm/s, surface recombination ceases to have an important effect on the cell efficiency. The optimum thickness decreases as the 7^{th} power of the temperature.

Although the optimum thickness of a bifacial cell is about twice the optimum thickness of a monofacial cell, there is still room to reduce the thickness of bifacial cells from the typical values found in commercial panels of about 160 μm without significant cost in output power. At a typical operating temperature of 45 °C the optimum thickness of a bifacial cell is 126 μm. Further reduction in thickness to 65 μm is possible with a 0.25% loss in relative efficiency. An advantage of thinner cells is that the temperature coefficient of the output power is smaller.

Finally, at room temperature under one sun illumination, the solar cell efficiency increases with illumination intensity at a rate of 5.88% (relative) per decade.

Appendix

In this appendix, we explain why the optimum thickness of the bifacial cell in Table II is twice the optimum thickness of the monofacial cell. The output power is the product of the output current and voltage. The current is proportional to the total electron-hole generation rate $G_1(L)$, which depends on cell thickness L, where the subscript 1 refers to a monofacial cell. According to (6), the voltage is proportional to $ln(n/n_{i,\text{eff}})$ where $n/n_{i,\text{eff}}$ is equal to the generation rate divided by thickness and a constant K, so that

$$P\left(L\right) G_1\left(L\right) ln\left(\frac{G_1\left(L\right)}{KL}\right) \tag{A1}$$

where P is the output power. In this expression, we have neglected the exponent in the argument that comes from the assumption that Auger recombination is the dominant loss mechanism. This simplifying assumption does not affect the argument. The value of the thickness $L = L_1$ for a monofacial cell which gives the maximum power can be found by setting the derivative of (A1) with respect to L equal to zero. In this case

$$\frac{G_1^{'}\left(L_1\right)}{G_1\left(L_1\right)} = \frac{1}{L_1\left(ln\left(\frac{G_1(L_1)}{KL_1}\right)+1\right)} \tag{A2}$$

where the prime indicates derivative, and the left-hand side is the fractional change in generation rate per unit thickness and the right-hand side is approximately the negative of the rate of change of voltage with respect to thickness. For a bifacial cell, we have the identical expression as in (A2) with all the subscripts 1 replaced by 2. We know that $G_2\left(L\right) = G_1\left(L/2\right)$, therefore, in the analogous equation to (A2) for the optimum thickness L_2 of bifacial cells we can replace G_2 with G_1 using the relation above, and with some rearranging we obtain

$$\frac{G_1^{'}\left(\frac{L_2}{2}\right)}{G_1\left(\frac{L_2}{2}\right)} = \frac{2}{L_2\left(ln\left(\frac{2G_1\left(\frac{L_2}{2}\right)}{KL_2}\right)+1-ln2\right)}. \tag{A3}$$

This is the same as (A2) except for the $ln2$ in the denominator. The first term in brackets in the denominator is equal to $V_{\text{oc}}/kT30$ which is large compared with $ln2$. If we neglect $ln2$ in (A3), with reference to (A2) we find that $L_2 = 2L_1$. In other words, the optimum thickness of the bifacial cell is approximately twice the optimum thickness of the monofacial cell.

This result can be further illustrated by choosing an explicit form for the generation rate as a function of thickness. The generation rate $G_1(L)$ goes to zero at small L and saturates at a constant value for large L. A mathematical expression with this behavior is

$$G_1\left(L\right) = \frac{aL}{1+aL}\ G_0 = G_2\left(2L\right). \tag{A4}$$

By substituting (A4) into (A2) and (A3), one obtains a relationship between the optimum thicknesses of the monofacial and bifacial cells. If V_{oc} is 761 meV and the optimum thickness of the monofacial cell is 100 μm then the optimum thickness of the bifacial cell is 195 μm, once again almost twice as thick as the monofacial cell, and in good agreement with the results in Table II above.

Acknowledgment

The authors would like to thank an anonymous Referee for pointing out an error in the manuscript and other useful suggestions.

References

[1] Bloomberg new energy finance. Accessed on: Sep. 2020, [Online]. Available: about.bnef.com/blog

[2] A. Richter, M. Hermle, and S. W. Glunz, "Reassessment of the limiting efficiency for crystalline silicon solar cells," *IEEE J. Photovolt.*, vol. 3, no. 4, pp. 1184–1191, Oct. 2013.

[3] S. Schäfer and R. Brendel, "Accurate calculation of the absorptance enhances efficiency limit of crystalline silicon solar cells with Lambertian light trapping," *IEEE J. Photovolt.*, vol. 8, no. 4, pp. 1156–1158, Jul. 2018.

[4] B. A. Veith-Wolf, S. Schäfer, R. Brendel, and J. Schmidt, "Reassessment of intrinsic lifetime limit in n-type crystalline silicon and implication on

maximum solar cell efficiency," *Sol. Energy Mater. Sol. Cells*, vol. 186, pp. 194–199, 2018.
[5] K. Yoshikawa *et al.*, "Silicon heterojunction solar cell with interdigitated back contacts for a photoconversion efficiency over 26%," *Nature Energy*, vol. 2, pp. 1–8, 2017, Art. no. 17032.
[6] M. A. Green *et al.*, "Solar cell efficiency tables (version 56)," *Prog. Photovolt. Res. Appl.*, vol. 28, pp. 629–638, 2020.
[7] G.-A. Migan, "Study of the operating temperature of a PV module," Project Rep. 2013 MVK160, May 16, 2013.
[8] G. Tamizhmani *et al.*, "Photovoltaic module thermal/wind performance: Long-term monitoring and model development for energy rating," in *Proc. NCPV Solar Program Rev. Meet.*, 2003, pp. 936–939.
[9] S. R. Wenham, M. A. Green, M. E. Watt, and R. Corkish, *Applied Photovoltaics*, 2nd ed. London, UK: Earthscan, 2007.
[10] Nominal Module Operating Temperature. Accessed on: Sep. 2020. [Online]. Available: www.canadiansolar.com
[11] C. D. Rodríguez-Gallegos *et al.*, "Monofacial vs bifacial Si-based PV modules: Which one is more cost effective?," *Solar Energy*, vol. 176, pp. 412–438, 2018.
[12] T. Tiedje, E. Yablonovitch, G. D. Cody and B. G. Brooks, "Limiting efficiency of silicon solar cells," *IEEE Trans. Electron Device*, vol. 31, no. 5, pp. 711–716, May 1984.
[13] E. Yablonovitch, "Statistical ray optics," *J. Opt. Soc. Amer.*, vol. 12, pp. 899–907, 1982.
[14] M. A. Green, "Lambertian light trapping in textured solar cells and light-emitting diodes: Analytical solutions," *Prog. Photovolt., Res. Appl.*, vol. 10, pp. 235–241, 2002.
[15] P. Sheng, "Optical absorption of thin film on a lambertian reflector substrate," *IEEE Trans. Electron Device*, vol. 31, no. 5, pp. 634–626, May 1984.
[16] M. Ernst and R. Brendel, "Lambertian light trapping in thin crystalline macroporous Si layers," *Phys. Status Solidi RRL*, vol. 8, pp. 235–238, 2014.
[17] S. Bhattacharya and S. John, "Beyond 30% conversion efficiency in silicon solar cells: A numerical demonstration," *Sci. Rep.*, vol. 9, 2019, Art. no. 12482. [Online]. Available: https://www.nature.com/articles/s41598-019-48981-w
[18] S. Bhattacharya, I. Baydoun, M. Lin, and S. John, "Towards 30% power conversion efficiency in thin-silicon photonic-crystal solar cells," *Phys. Rev. Appl.*, vol. 11, pp. 014005-2351–014005-26, 2019.
[19] K. G. Svantesson and N. G. Nilsson, "Determination of the temperature dependence of the free carrier and interband absorption in silicon at 1.06 μm," *J. Phys. C, Solid State Phys.*, vol. 12, pp. 3837–3842, 1979.
[20] S. C. Baker-Finch, K. R. McIntosh, D. Yan, K. C. Fong, and T. C. Kho, "Near-infrared free carrier absorption in heavily doped silicon," *J. Appl. Phys.*, vol. 116, pp. 063106-2351–063106-12, 2014.
[21] P. P. Altermatt, A. Schenk, F. Geelhaar, and G. Heiser, "Reassessment of the intrinsic carrier density in crystalline silicon in view of band-gap narrowing," *J. Appl. Phys.*, vol. 93, pp. 1598–1604, 2003.
[22] T. Trupke *et al.*, "Temperature dependence of the radiative recombination coefficient of intrinsic crystalline silicon," *J. Appl. Phys.*, vol. 94, no. 8, pp. 4930–4937, 2003.
[23] W. Bludau, A. Onton, and W. Heinke, "Temperature dependence of the band gap of silicon," *J. Appl. Phys.*, vol. 45, no. 4, pp. 1846–1848, 1974.
[24] A. Wolf *et al.*, "Comprehensive analytical model for locally contacted rear surface passivated solar cells," *J. Appl. Phys.*, vol. 108, pp. 1–13, 2010.
[25] A. Schenk, "Finite-temperature full random-phase approximation model of band gap narrowing for silicon device simulation," *J. Appl. Phys.*, vol. 84, no. 7, pp. 3684–3695, 1998.
[26] A. Richter, J. Benick, M. Hermle, and S. W. Glunz, "Excellent silicon surface passivation with 5 Å thin ALD Al_2O_3 layers: Influence of different thermal post-deposition treatments," *Phys. Status Solidi RRL*, vol. 5, no. 5/6, pp. 202–204, 2011. doi: 10.1002/pssr.201105188.
[27] A. Richter, S. W. Glunz, F. Werner, J. Schmidt, and A. Cuevas, "Improved quantitative description of auger recombination in crystalline silicon," *Phys. Rev. B*, vol. 86, pp. 165202-2351–165202-14, 2012.
[28] K. A. Colletta *et al.*, "An enhanced alneal process to produce SRV$<$1 cm/s in 1 Ω cm n-type Si," *Sol. Energy Mater. Sol. Cells*, vol. 173, pp. 50–58, 2017.
[29] G. Dingemans and W. M. M. Kessels, "Status and prospects of Al_2O_3-based surface passivation schemes for silicon solar cells," *J. Vacuum Sci. Technol. A*, vol. 30, no. 4, pp. 040802-2351–040801-27, Jul./Aug. 2012.
[30] R. S. Bonilla, B. Hoex, P. Hamer, and P. R. Wilshaw, "Dielectric surface passivation for silicon solar cells: A review," *Phys. Status Solidi A*, vol. 214, pp. 1–30, 2017, Art. no. 1700293. doi: 10.1002/pssa.201700293.
[31] R. S. Bonilla, C. Reichel, M. Hermle, and P. R. Wilshaw, "Extremely low surface recombination in 1 Ω cm n-type monocrystalline silicon," *Phys. Status Solidi RRL*, vol. 11, pp. 1–5, 2017, Art. no. 1600307. doi: 10.1002/pssr.201600307.
[32] J. Haschke, O. Dupré, M. Boccard, and C. Ballif, "Silicon heterojunction solar cells: Recent technological development and practical aspects—from lab to industry," *Sol. Energy Mater. Sol. Cells*, vol. 187, pp. 140–153, 2018.
[33] S. Wang and D. Macdonald, "Temperature dependence of auger recombination in highly injected crystalline silicon," *J. Appl. Phys.*, vol. 112, no. 11, pp. 113708-2351–113708-2354, 2012.
[34] M. Rosling, H. Bleichner, P. Jonsson, and E. Nordlander, "The ambipolar diffusion coefficient in silicon: Dependence on excess-carrier concentration and temperature," *J. Appl. Phys.*, vol. 76, no. 5, pp. 2855–2859, Sep. 1994.
[35] M. A. Green, "Self-consistent optical parameters of intrinsic silicon at 300 k including temperature coefficients," *Sol. Energy Mater. Sol. Cells*, vol. 92, no. 11, pp. 1305–1310, 2008.
[36] H. T. Nguyen, F. E. Rougieux, B. Mitchell, and D. Macdonald, "Temperature dependence of the band-band absorption coefficient in crystalline silicon from photoluminescence," *J. Appl. Phys.*, vol. 115, pp. 043710-2351–043710-2358, 2014.
[37] H. Schlangenotto, H. Maeder, and W. Gerlach, "Temperature dependence of the radiative recombination coefficient in silicon," *Phys. Stat. Sol.*, vol. 21, pp. 357–367, 1974.
[38] P. P. Altermatt *et al.*, "Injection dependence of spontaneous radiative recombination in c-Si: Experiment, theoretical analysis and simulation," in *Proc. 5th Int. Conf. Num. Simul. Optoelectron. Devices*, 2005, pp. 47–48.
[39] P. Würfel, "The chemical potential of radiation," *J. Phys. C, Solid State Phys.*, vol. 15, pp. 3967–3985, 1982.
[40] O. D. Miller, E. Yablonovitch, and S. R. Kurtz, "Strong internal and external luminescence as solar cells approach the Shockley–Queisser limit," *IEEE J. Photovolt.*, vol. 2, no. 3, pp. 303–311, Jul. 2012.
[41] Standard Tables for Reference Solar Spectral Irradiances, in *Direct Normal and Hemispherical on 37° Tilted Surface*. West Conshohocken, PA, USA: ASTM International (2012). doi: doi.org/10.1520/G0173-03R12.
[42] International Technology Roadmap for Photovoltaic, Accessed on: Sep. 2020. [Online]. Available: itrpv.vdma.org
[43] M. Kasu *et al.*, "Temperature dependence measurements and performance analyses of high-efficiency interdigitated back-contact, passivated emitter and rear cell, and silicon heterojunction photovoltaic modules," *Jpn. J. Appl. Phys.*, vol. 57, no. 8S3, 2018, Art. no. 08RG18. doi: 10.7567/JJAP.57.08RG18.
[44] T. Tiedje and D. A. Engelbrecht, "Temperature dependence of the limiting efficiency of bifacial silicon solar cells," in *Proc. 47th IEEE Photovolt. Spec. Conf.*, 2020.
[45] V. Bahrami-Yekta and T. Tiedje, "Limiting efficiency of indoor silicon photovoltaic devices," *Opt. Express*, vol. 26, no. 22, pp. 28238–28248, 2018.